



Experimental study on the effect of the milling condition of an aluminum alloy on subsurface residual stress

Chieko Kuji¹ · Christopher R. Chighizola² · Michael R. Hill² · Jan C. Aurich³ · Hitoshi Soyama¹

Received: 16 April 2023 / Accepted: 7 July 2023 / Published online: 14 July 2023
© The Author(s) 2023

Abstract

Aluminum alloys used in monolithic parts for aerospace applications are subjected to distortion and residual stress (RS) generated by milling, affecting the product fatigue life. Particularly, the change in RS with depth (z) has a characteristic distribution with a maximum compressive RS at a z several tens of micrometers from the surface; however, the RS value depends on the measurement method used. In this study, the RS distribution with z from the surface after milling was measured for the AA7050-T7451 aluminum alloy by two-dimensional X-ray diffraction (2D method). The results were compared with those of four prior measurement methods, and the validity of 2D method was verified. The changes in subsurface RS with z showed similar distributions under all measurement conditions except when $\cos(\alpha)$ -XRD was employed. The 2D method provides high repeatability. The in-plane RS distribution was also measured using 2D method to investigate the effect of milling conditions on this distribution. The RS values varied markedly depending on the measurement position, particularly at a small collimator diameter of 0.146 mm, allowing detection of localized extreme RS values. The maximum RS at $z=0$ mm was -85.6 MPa at a cutting speed of $v_c=200$ m/s and feed per tooth of $f_z=0.05$ mm, while it was -16 MPa for $v_c=450$ m/s and 6.8 MPa for $f_z=0.2$ mm, revealing that the compressive RS changes to tensile RS as v_c and f_z increase.

Keywords Residual stress measurement · Surface roughness · Machining · Milling · X-ray diffraction · Aluminum alloy

1 Introduction

Monolithic structural components are widely used in aircraft manufacturing and require light products, short assembly times, high production efficiencies, and low production costs [1]. Aluminum alloys are used as monolithic components for aerospace applications owing to their low cost, high specific strength, low density, good thermal conductivity, corrosion resistance, and other material properties that facilitate the formation of complex shapes [2, 3]. Such monolithic parts are fabricated using machining techniques, such as milling. Milling is a cutting process that removes workpiece material by pressing a rotating blade against a fixed workpiece, thereby achieving high machining efficiency because a wide area can be removed simultaneously. Moreover, milling can be used for almost all materials [4], and high surface quality can be obtained, even for high-strength, difficult-to-machine materials [5]. However, the thinness and large size of aircraft aluminum alloy parts reduce their rigidity, and high material removal of as much as 90% causes residual stress (RS) on the machined surface, which easily results in distortion [1, 6]. The distortion and RS caused by milling can also reduce

✉ Chieko Kuji
c-kuji@tohoku.ac.jp

Christopher R. Chighizola
crchighizola@ucdavis.edu

Michael R. Hill
mrhill@ucdavis.edu

Jan C. Aurich
fbk@mv.uni-kl.de

Hitoshi Soyama
soyama@mm.mech.tohoku.ac.jp

¹ Department of Finemechanics, Tohoku University, 6-6-01 Aoba, Aramaki, Aoba-Ku, Sendai 980-8579, Japan

² Department of Mechanical and Aerospace Engineering, University of California, Davis, One Shields Ave, Davis, CA 95616, USA

³ Institute for Manufacturing Technology and Production Systems, RPTU Kaiserslautern, 67653 Kaiserslautern, Germany

fatigue life [7]. Aircraft manufacturers are estimated to incur hundreds of millions of dollars or more in economic losses owing to scrap materials and rework related to such component distortions [8]. Therefore, to improve aircraft safety, optimize manufacturing, and reduce costs, it is necessary to clarify the causes of RS.

Pioneering studies have attempted to derive the RS distribution with depth (z) in the milled surface region using the electrolytic etching-deflection technique [9]. In recent years, researchers have experimentally confirmed that the maximum compressive RS arises at a z near the surface and that RS gradually decreases with increasing z [10–12]. Such a z -directed RS distribution is called a “root” ($\sqrt{\quad}$) shape [1]. Feng et al. used numerical analysis to obtain the RS distribution with z of milling and showed that the distribution is $\sqrt{\quad}$ -shaped [13, 14], similar to prior experimental results [1, 9, 10, 12]. The z range of the compressive RS and the z and magnitude of the maximum compressive RS in the near-surface RS distribution vary depending on milling parameters, such as cutting speed (v_c), feed per tooth (f_z), and z of the cut [15–17]. Tensile RS in metallic materials accelerates fatigue crack propagation, whereas compressive RS inhibits crack propagation [18]. For example, in trochoidal milling [19], the cutting tool is moved in a spiral motion to maintain the cutting rate and reduce the cutting resistance and RS. However, because compressive RS plays a role in suppressing fatigue failure, it is not necessarily preferable to reduce the RS. Therefore, clarifying the milling parameters that affect the degree of tensile/compressive RS in the milled material can improve the fatigue life and reduce the product cost. However, when the RS is measured experimentally, it can vary significantly depending on the measurement method, even under the same milling conditions.

Several experimental methods exist for measuring RS [20]. Hole-drilling and slotting methods are commonly used as mechanical measurement methods, whereas X-ray diffraction (XRD) methods are X-ray-based and can be further divided into $\sin^2(\psi)$, $\cos(\alpha)$, and two-dimensional (2D) methods, depending on the measurement technique. For example, XRD has recently been used to measure the RS in austenitic stainless steels treated at cryogenic temperatures [21]. Vrabel et al. measured the RS distribution with z of Inconel 718 after using the $\sin^2(\psi)$ and hole-drilling methods [22]. However, they used the $\sin^2(\psi)$ method for the top surface and the hole-drilling method to measure the RS distribution with z but did not compare measurement methods [22]. Bordinassi et al. compared the surface RS after milling measured using the blind hold method (a mechanical measurement method) with that measured using the $\cos(\alpha)$ method; however, they did not compare the z RS distributions [23]. Chighizola et al. mentioned the lack of a systematic comparison of these measurement methods and conducted z RS distribution measurements of milled aluminum

using the hole-drilling, slotting, $\sin^2(\psi)$ and $\cos(\alpha)$ methods [24]. Consequently, although hole-drilling requires measurement skills, the results with the highest repeatability were obtained at a z of 0.03 mm or greater, whereas the results obtained using the $\cos(\alpha)$ method disagreed with the other measurement results. In contrast, the 2D method, which, like the $\cos(\alpha)$ method, has a 2D detector, has been shown to have higher measurement accuracy than the $\sin^2(\psi)$ method, which is mostly used for RS measurements in laboratories [25]. RS can be measured in submillimeter areas using a collimator [25]. Therefore, the validity of the 2D method can be investigated by comparing the measurement results with those of the hole-drilling, slotting, $\sin^2(\psi)$ and $\cos(\alpha)$ methods [24]. In addition, if large differences resulting from milling exist in the RS distribution in the plane direction, they will distort the machined parts. However, few studies have investigated the distribution of RS on machined surfaces in detail.

In this study, RS measurements using the 2D method were performed on the same samples as those in [24], an aluminum alloy (AA7050-T7451), after milling, to investigate the validity of the 2D method. Furthermore, the in-plane RS distribution, which has not been investigated experimentally or analytically, was evaluated using the 2D method. First, the RS distribution with z was investigated and compared with the major RS measurement methods (hole-drilling, slotting, $\sin^2(\psi)$, and $\cos(\alpha)$ methods), and the measurement accuracy was evaluated. Subsequently, the 2D method was used to precisely measure the distribution of RS with z in the in-plane direction, and the effect of the milling conditions on the subsurface RS was investigated.

2 Materials and methods

2.1 Workpiece material and milling conditions

A common aerospace aluminum sheet (AA7050-T7451) with a thickness of 25 mm was used as the experimental material, and the samples were prepared as previously described [24]. The AA7050-T7451 standard is defined in AMS4050, and AA indicates that this material was provided by Aluminum Association, Inc. Aluminum 7050 has high strength coupled with high resistance to exfoliation corrosion and stress corrosion cracking, high fracture toughness, and fatigue resistance. T7451 indicates that this material was solution-annealed and the RS was removed and further overaged. A milling machine (DMU 70 CNC, DMG Mori Co., Ltd.) and a cemented carbide end mill (F3AA1200AWL, Kennametal, Inc.) were used. Figure 1a shows a schematic of the milling parameters, Fig. 1b shows a photograph of the experimental setup [26], and Fig. 1c shows the layout of the measurement workpiece.

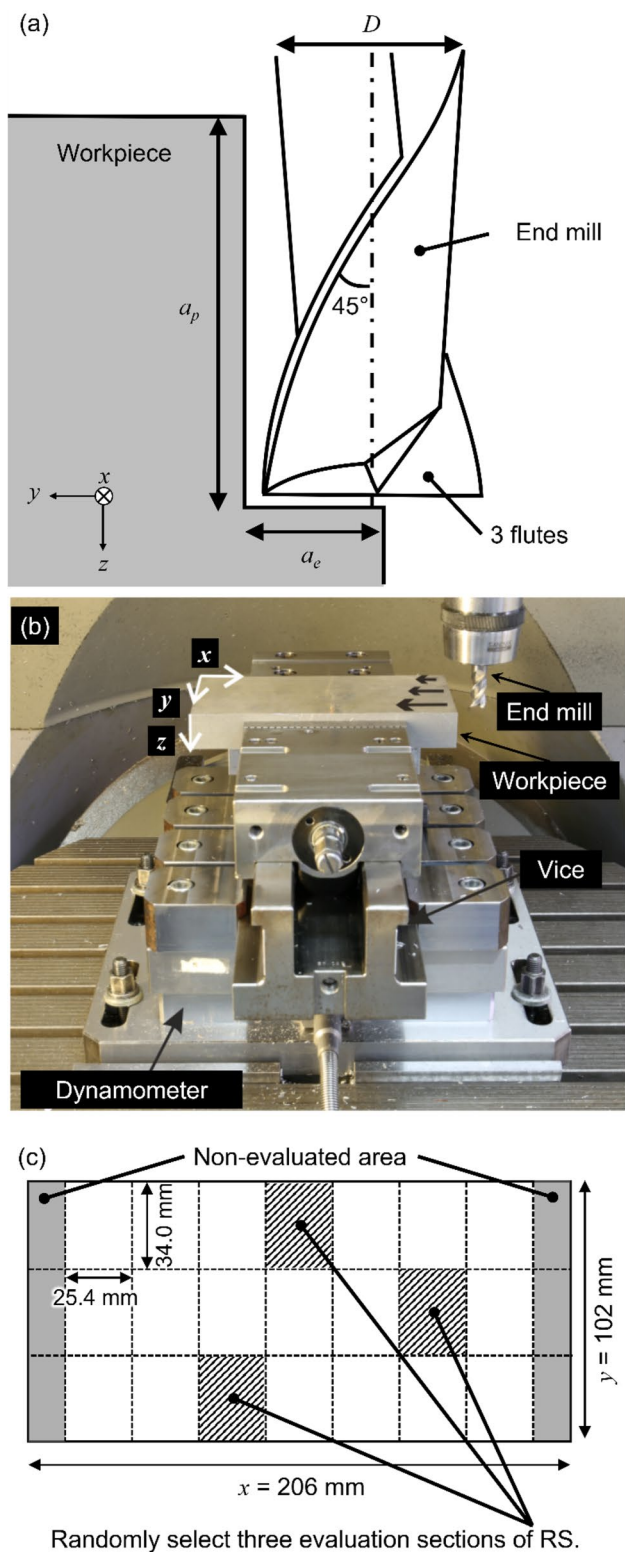


Fig. 1 a Schematic of the milling parameters, b photograph of the experimental setup [26], and c layout of the measurement workpiece

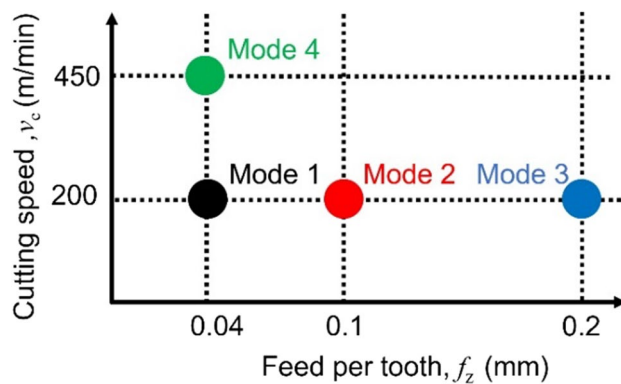


Fig. 2 Schematic of the milling conditions [24]

As shown in Fig. 1a and b, the x -, y -, and z -axes are defined as the length, width, and thickness directions of the sample, and the workpiece sizes are 206, 106, and 28 mm. The tool was a square with a diameter $D = 12$ mm and three cutting edges with a torsional angle of 45° (Fig. 1a). The z of cut a_p and width of cut a_e were set to 3 and 4 mm, respectively. The workpiece was fixed using a vice, and a piezoelectric dynamometer was used to record the milling forces (Fig. 1b). As shown in Fig. 1c, the milled workpieces were subdivided into area grids of $x = 25.4$ mm and $y = 34.0$ mm. RS was measured near the center of the grids. Three measurement areas were randomly selected, and the repeatability of each RS measurement method was investigated. Four conditions were set for v_c and f_z (Fig. 2).

The effect of f_z on RS was examined by changing f_z to 0.04, 0.10, and 0.20 mm with $v_c = 200$ m/min for Modes 1–3, and the effect of v_c on RS was also examined by changing v_c to 200 and 400 m/min with $f_z = 0.04$ mm for Modes 1 and 4. The specific milling procedure was as follows. Beginning at the milling origin, the tool was cut to a_p in the positive direction of the z -axis and a_p in the positive direction of the y -axis and then scanned 200 mm toward the negative direction of the x -axis. This operation was defined as a single path. After completing one path, the tool was returned to the machining origin along the x -axis and offset by a_e along the y -axis; the same path was repeated. Milling was completed when a total of 100 mm was cut in the y -direction. Material from the same lot was used for each milling process. As the milling area is sufficiently large for v_c and f_z , the repeatability of each measurement method can be evaluated by markedly changing the measurement area, as shown in Fig. 1c. The machined surface was observed via scanning electron microscopy (SEM; JCM-7000, JEOL, Ltd.), and the surface profile was measured using a contact-type surface roughness meter.

2.2 RS measurement methods

RS was measured using 2D method and compared with results of the hole-drilling, slotting, $\sin^2(\psi)$, and $\cos(\alpha)$ methods [24]. These measurement methods are briefly described below:

(i) The hole-drilling method, as specified in ASTM E837-20, calculates the RS from the three-directional strain generated by the stress release. In this approach, holes are drilled incrementally at the centers of the rosette strain gauges placed on the specimen [27].

(ii) The slotting method is similar to the one-dimensional (1D) hole-drilling method. A single component of RS can be measured from the strain generated in a uniaxial strain gauge by cutting a long, narrow groove perpendicular to the direction of the RS to be measured [28, 29].

(iii) The $\sin^2(\psi)$ method is a basic RS measurement technique that uses XRD. This is performed using a zero-dimensional or 1D detector [30, 31]. First, the lattice plane spacing d is derived from the diffraction angle 2θ when X-rays are incident at various angles ψ . The residual strain calculated from d is plotted against $\sin^2\psi$ to obtain the slope of the regression line. RS can be calculated by multiplying the slope by the elastic constant ($1/2 S_2$) of the lattice plane.

(iv) The $\cos(\alpha)$ method employs a 2D detector to detect a single incident X-ray beam and determine the RS from the obtained Debye–Scherrer rings [32]. Based on an unstressed sample, the strain with respect to the center angle α of the Debye–Scherrer ring can be determined, and RS can be calculated from the slope of the strain with respect to $\cos(\alpha)$.

The hole-drilling and slotting methods have the advantages of being fast, easy to use, and portable. However, they have the disadvantages of data interpretation and limited strain sensitivity and resolution [33]. The $\sin^2(\psi)$ and $\cos(\alpha)$ methods have the advantages of the ability to measure a wide range of materials and the possibility of measuring macro- and micro-RSs; their disadvantages include the use of laboratory-based systems and small components and only providing basic measurements [33]. In each method, the material is incrementally

removed from the surface, and measurements are taken at each step to obtain a RS profile from the surface to z .

The 2D method involves using a 2D detector. However, the stress components are obtained by applying X-rays from various directions using the least squares method [34]. The left image in Fig. 3 shows the XRD system configuration, and the right image shows the coordinate system of the measured sample.

The sample was irradiated with X-rays from various incident directions by adjusting φ , ψ , and ω , as shown in Fig. 3, and some of the Debye rings, which were diffraction patterns generated from the sample, were detected using a 2D position-sensitive proportional counter (2D-PSPC). RS was obtained by measuring the diffraction angle 2θ at each position in the χ -direction ($\chi = 90^\circ - \psi$). If the stress in the j -direction relative to the i -plane is σ_{ij} , then all stress components in the sample coordinate system are expressed as in Eq. (1), and each stress component can be measured using the least squares method [34]. In Eq. (1), f_{ij} is a function of ψ , φ , ω , χ , and θ and can be obtained from Eqs. (2)–(8) [34].

$$f_{xx}\sigma_{xx} + f_{xy}\sigma_{xy} + f_{yy}\sigma_{yy} = \ln\left(\frac{\sin\theta_0}{\sin\theta}\right) \quad (1)$$

$$f_{xx} = A^2, f_{xy} = 2AB, f_{yy} = B^2 \quad (2)$$

$$A = a\cos\phi - b\cos\psi\sin\phi + c\sin\psi\sin\phi \quad (3)$$

$$B = a\sin\phi + b\cos\psi\cos\phi - c\sin\psi\cos\phi \quad (4)$$

$$C = b\sin\psi + c\cos\psi \quad (5)$$

$$a = \sin\theta\cos\omega + \sin\chi\cos\theta\sin\omega \quad (6)$$

$$b = -\cos\chi\cos\theta \quad (7)$$

$$c = \sin\theta\sin\omega - \sin\chi\cos\theta\cos\omega \quad (8)$$

Fig. 3 Schematic of the XRD system and sample coordinates

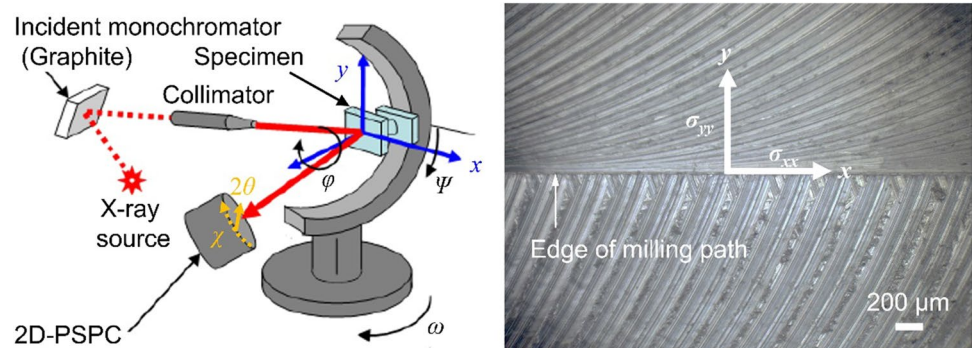


Table 1 Measurement conditions for the 2D method

φ -direction (deg.)	0, 45, 90, 135, 180, 225, 270, 315
ψ -direction (deg.)	0, 30, 60
ω -direction (deg.)	107–115

Table 2 Analyzed areas of the obtained XRD pattern using the 2D method (Debye ring)

2θ -direction (deg.)	135–145
χ -direction (deg.)	65–115

As shown in Fig. 3 (right), the y -axis origin was set as the edge of each milling path, and the x - and y -axes were set in the length and width directions of the sample, respectively.

2.3 Conditions for measuring the RS distribution with z

An X-ray diffractometer (D8 Discover, Bruker Corp.) and 2D-PSPC (V500, Bruker Corp.) were used for the RS measurements, and the RSs were calculated using LEP-TOS software (version 7.9, Bruker Japan K. K.). The X-ray source was Cr- $K\alpha$ radiation (wavelength 2.29093 Å, 35 kV, 40 mA). The samples were irradiated with X-rays after narrowing the beam diameter using a collimator diameter (d_c) to 0.8 mm. The exposure time per frame was set to 20 s. Table 1 lists the measurement conditions for the 2D method.

Eight conditions were applied in the φ -direction (0–315°) and three in the ψ -direction (0°, 30°, and 60°), and 24 frames were measured while swinging in the ω -direction from 107° to 115°. During the measurement, the sample stage was scanned within ± 2 mm in the x - and y -directions, and diffraction information was obtained for each 4 mm \times 4 mm area. Table 2 lists the analyzed areas of the Debye ring.

The RS was calculated using the diffraction angles from the Al [311] plane by analyzing the Debye rings in the range of 135–145° in the 2θ -direction and 65–115° in the χ -direction. The change in the RS distribution with z was obtained by gradually removing the material surface by electropolishing and measuring the stress in the exposed plane. Phosphoric acid with water and aluminum was used as the electropolishing fluid, and the removal z was measured after each electropolishing using a micrometer. The etch pit was rectangular with an in-plane area of $x = 3$ mm \times $y = 8$ mm. The RS versus z profile was measured at three different locations along x for $y = 0$, as was done in a previous study [24], and the average of the three z profiles and the standard deviations at each z were compared to the prior results [24]. No z correction was performed, and raw XRD data were used.

2.4 Conditions for measuring the RS distribution in plane

Two collimators with $d_c = 0.8$ and 0.146 mm were used to measure the RS distribution in the plane direction of the sample. For the $d_c = 0.8$ - and 0.146-mm collimators, the exposure times per frame were set to 40 s and 20 min, respectively. The measurement conditions were the same as those listed in Table 1, and 24 frames were used. During the measurements, the sample stage was not scanned; however, a fixed-point area was measured. These measurements were repeated at different locations in the range of -2 mm $\leq y \leq 2$ mm, and the RS distribution in the y -axis direction in the xy -plane was measured at 9 and 17 points at equal intervals for the collimators with $d_c = 0.8$ and 0.146 mm, respectively. The analysis range of the Debye ring was set as listed in Table 2, and the RSs were calculated using the procedure described in Sect. 2.3. This measurement was performed for each z within an area of $x = 3$ mm \times $y = 8$ mm, achieved by electropolishing as described in Sect. 2.3.

3 Results and discussion

3.1 Evaluation of the machined surface

Figure 4 shows an SEM image of the milled surface and surface roughness profile in the y -axis direction. Figure 4a–d correspond to Modes 1–4, respectively.

The maximum height roughness (R_z) of Modes 1–4 were 3.7, 9.9, 25.1, and 7.3 μm , and the arithmetical mean heights (R_a) were 0.7, 1.8, 3.1, 1.1 μm , respectively. In this study, a_e was set to 4 mm, and each profile indicated that the surface geometry changed every 4 mm. Figure 4a–c, corresponding to Modes 1–3 with $v_c = 200$ m/min, show that the R_z and R_a increased as f_z increased, and the R_z and R_a values of Mode 3 (Fig. 4c) were approximately 6.8 and 4.4 times higher, respectively, than those in Mode 1 (Fig. 4a). The f_z value of Mode 3 is five times greater than that of Mode 1. R_z and R_a were used to evaluate the projection and average surface characteristics, respectively. Both roughness values increased significantly with increasing f_z . Next, by comparing Mode 1 in Fig. 4a and Mode 4 in Fig. 4d with different values of v_c , the v_c in Mode 4 was found to be 2.25 times greater than that in Mode 1, and R_z and R_a were 2.0 and 1.6 times greater, respectively. Considering the increased rate of surface roughness with respect to each parameter value, f_z had a greater influence on the surface roughness than v_c . Although milling conditions with small f_z and v_c are desirable for high surface accuracy, the machining efficiency can be improved by increasing f_z and v_c . Furthermore, the milling

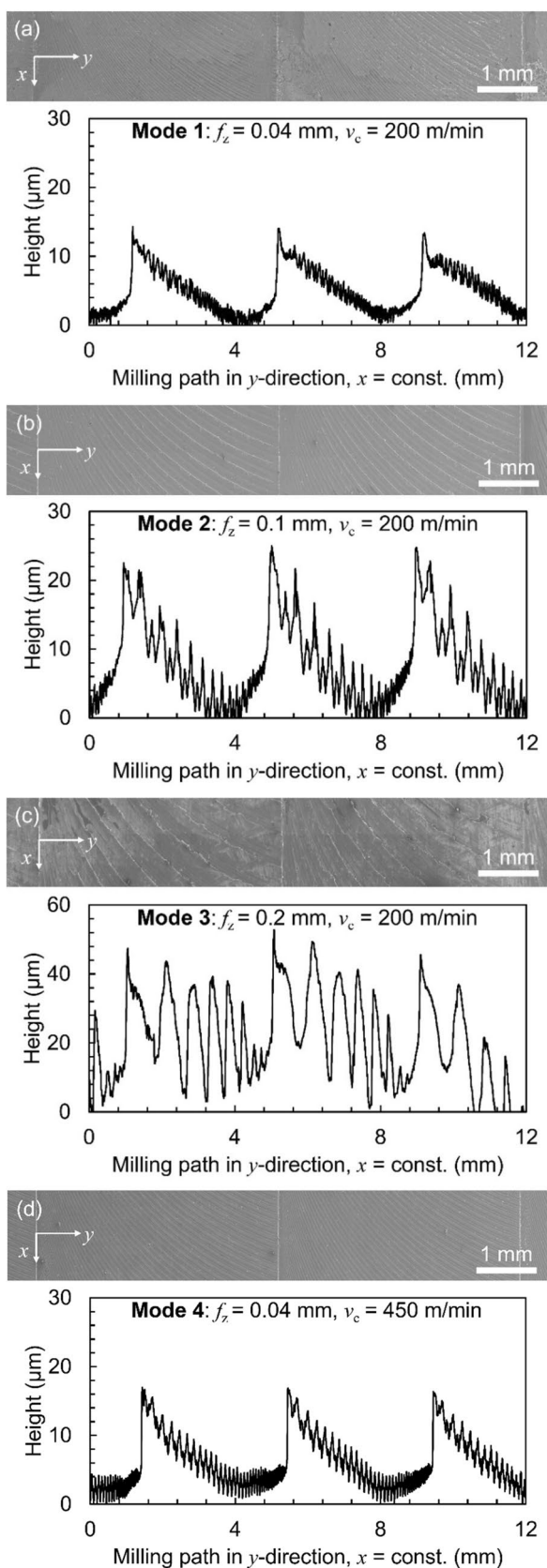


Fig. 4 SEM images and surface roughness profiles of the milled surfaces: **a** Mode 1, **b** Mode 2, **c** Mode 3, and **d** Mode 4

conditions should be determined by considering the effects of f_z and v_c on the tensile RS that causes fatigue cracks.

3.2 Evaluation of measurement accuracy of the 2D method

The RS of the milled samples with z under the same conditions was compared with the results of the hole-drilling, slotting, $\sin^2(\psi)$, and $\cos(\alpha)$ methods [24] to assess the measurement accuracy of the RS from the 2D method. However, the measurement positions differed slightly with z for each sample. Therefore, the constant z RS values were interpolated using the respective measurement results, and the interpolated values were compared.

Figure 5 shows the RS distribution with z , as measured using each measurement method. The results show σ_{yy} stress components milled in Mode 3. The three different RS measurements are indicated by the open symbols (triangles, squares, and diamonds). As shown in Fig. 1c, three different points on one sample were randomly selected for RS measurements with z . The average RS obtained by interpolation from each of the three measurement results is indicated by closed-color symbols, and the error bars indicate the standard deviations.

In Fig. 5a–e, the results, other than those of the $\cos(\alpha)$ method, show a $\sqrt{\quad}$ -shaped RS distribution. During milling, the tool and workpiece rub against each other, introducing a large RS near the milled surface. Because the material was heat-treated to remove RS before milling, the RS approached zero away from the milled surface. Therefore, the RS distribution with z became the $\sqrt{\quad}$ shape. The maximum RSs values at the interpolated z obtained using each measurement method are shown in Fig. 5f. The maximum compressive RS was at $z=0.055$ mm for the slotting and 2D methods, $z=0.041$ mm for the hole-drilling method, $z=0.028$ mm for the $\sin^2(\psi)$ method, and $z=0.015$ mm for the $\cos(\alpha)$ method. Focusing on repeatability, the standard deviations of the mechanical measurement methods—the hole-drilling and slotting methods (Fig. 5a and b) were larger near the surface but became smaller as the measurement position became deeper. In particular, the hole-drilling method resulted in almost no measurement errors at $z > 0.03$ mm. Specifically, the standard deviations of the $\sin^2(\psi)$ and 2D methods at $z=0.005$ mm were 1% and 8% of those of the hole-drilling method, respectively. In contrast, for the XRD methods (the $\sin^2(\psi)$, $\cos(\alpha)$, and 2D methods; see Fig. 5c–e, respectively) the $\cos(\alpha)$ method resulted in a large standard deviation at all measured z values, whereas the $\sin^2(\psi)$ and 2D methods resulted in small standard deviations at all z values.

In Fig. 6, the interpolated values obtained from Fig. 5 are compared. The standard deviations are shown as error bars. Figure 6a shows the RS distribution obtained from each measurement method with z ; all the interpolated values

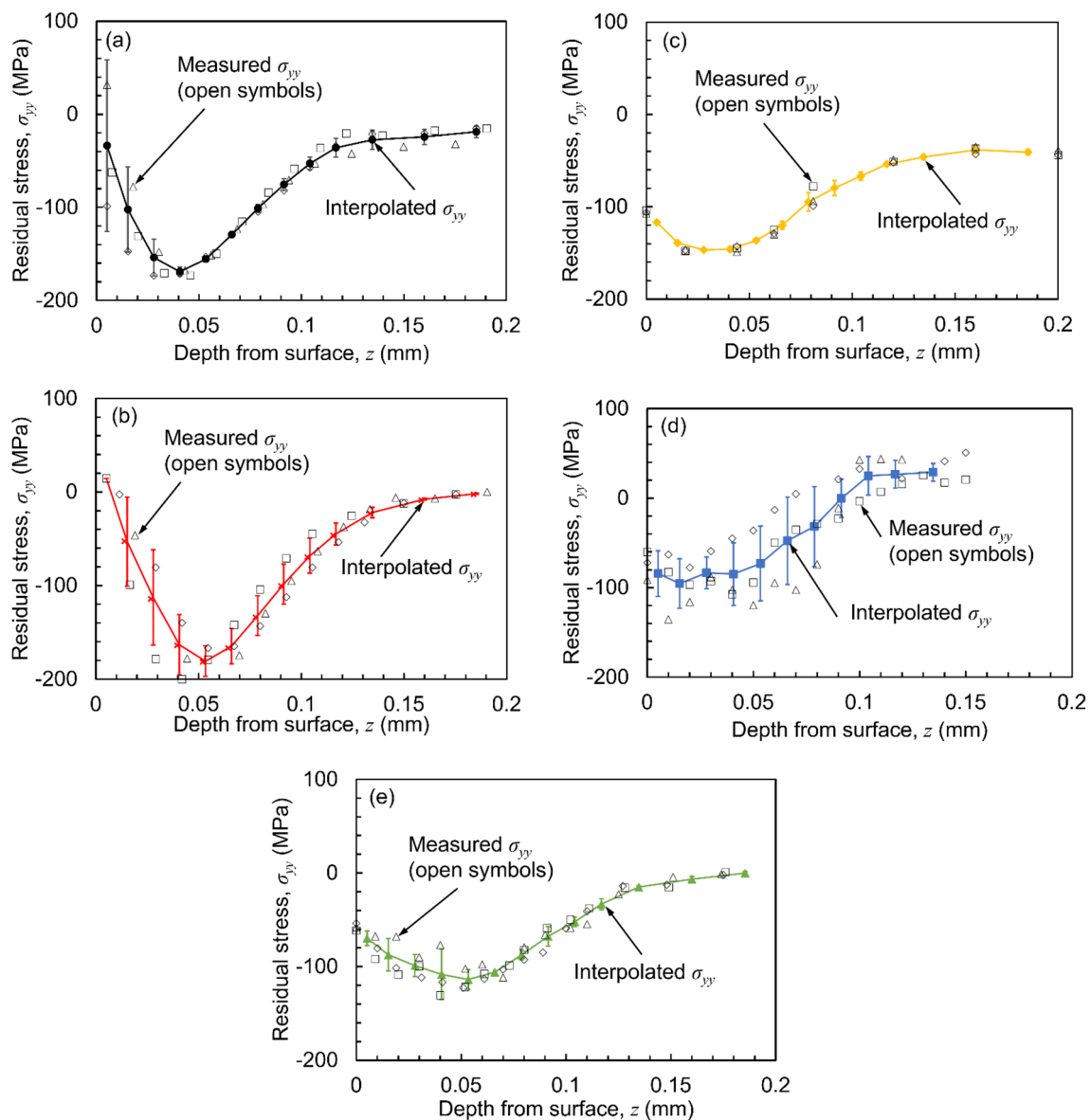


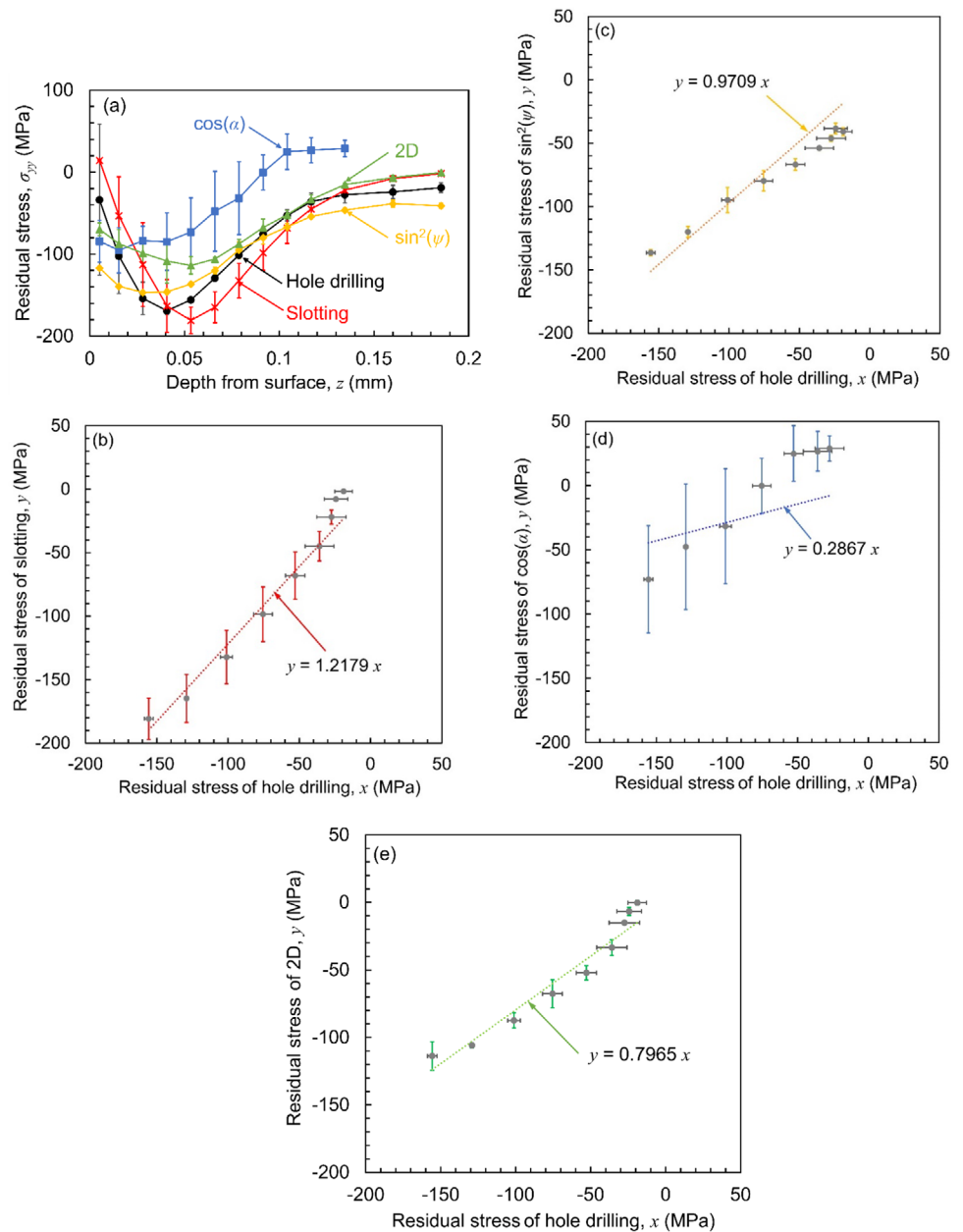
Fig. 5 RS measured using each method and interpolated values: **a** hole-drilling, **b** slotting, **c** $\sin^2(\psi)$, **d** $\cos(\alpha)$, and **e** 2D methods; **f** shows the maximum RSs at the interpolated z values obtained from each method

represent the RS at the same z . Figure 6b–e show the RS at the same z plotted with the results of the hole-drilling method on the horizontal x -axis and those of the other methods on the vertical y -axis.

In a previous study [24], the highest repeatability was obtained using the hole-drilling method compared with those using the slotting, $\sin^2(\psi)$, and $\cos(\alpha)$ methods. Therefore, repeatability was evaluated by comparing the respective measurement results with those of the hole-drilling method. Specifically, Fig. 6b–e show the measurement results of the slotting, $\sin^2(\psi)$, $\cos(\alpha)$, and 2D methods, respectively, compared with those of the hole-drilling method. However, the standard deviation from using the hole-drilling method near

the surface was large; therefore, the values of $z \geq 0.05334$ mm were compared. The correlation coefficients for the results shown in Fig. 6b–e are 0.982, 0.895, 0.657, and 0.973, respectively, and the uncorrelated probabilities are 0.0003, 0.11, 10.9, and 0.0011%, respectively. Thus, the 2D method results are highly positively correlated with the results of the hole-drilling method. By contrast, the slopes of the regression lines in Fig. 6b–e are 1.2179, 0.9709, 0.2867, and 0.7965, respectively. Hence, the $\sin^2(\psi)$ method was the most consistent with the absolute RS value of the hole-drilling method. However, the $\sin^2(\psi)$ method provides only partial diffraction information from Debye rings and determines the RS values by linear regression between two parameters obtained from a certain

Fig. 6 Comparison of measured RSs. **a** RSs obtained by interpolation from all methods at different z values (horizontal x -axis) and RSs from the **b** slotting method, **c** $\sin^2(\psi)$ method, **d** $\cos(\alpha)$ method, and **e** 2D method (vertical y -axis) as a function of RSs from hole drilling (horizontal x -axis)



diffraction angle 2θ ; thus, the accuracy of the regression line directly affects the stress measurement results [35]. If the target material and determination method of the 2θ value are not optimized, the measurement error is extremely large [35], and the 2D method has a smaller repetitive measurement error [25]. Therefore, the $\sin^2(\psi)$ method is effective if the material and 2θ value conditions are satisfied to increase the degree of regression linearity for determining RS. The 2D method obtains diffraction information from a wide range of Debye rings by using a 2D detector to determine the RS and obtain results with high repeatability. Although there is a slight difference (approximately 50 MPa at the maximum compressive RS) from the absolute value measured using the hole-drilling

method, it is possible to perform highly accurate measurements with a small error, even in the near-surface area where the mechanical measurement is unsatisfactory. Repeatability is important when evaluating RS distribution trends. The 2D method, in which the measurement area can be selected only by changing the collimator diameter, is extremely effective for measuring the RS in a local area.

3.3 Effects of milling parameters on the RS distribution with z using the 2D method

Figure 7a–d show the RS distribution changes with z measured using the 2D method for the milled samples under

Modes 1–4. The milling tool was scanned in the x -axis positive direction, and σ_{xx} , σ_{yy} , and σ_{xy} were the RS components in the x -, y -, and shear directions, respectively. The standard deviations are shown as error bars.

To investigate the effect of f_z , the RS distributions of Modes 1–3 were compared, as shown in Fig. 7a–c, in which v_c was constant at 200 m/min and only f_z was changed. The z ranges of RS in all RS components were $z \leq 0.06$ mm for Mode 1 with $f_z = 0.04$ mm, as shown in Fig. 7a, $z \leq 0.08$ mm for Mode 2 with $f_z = 0.1$ mm, as shown in Fig. 7b, and $z \leq 0.13$ mm for Mode 3 with $f_z = 0.2$ mm, as shown in Fig. 7c, indicating that the larger the f_z , the deeper the RS. The compressive RS peaks in the $\sqrt{\quad}$ shape for σ_{xx} and σ_{yy} occurred at greater z values as f_z increased, with peaks for σ_{xx} in Modes 1–3 at -112.1 ± 6.7 MPa at $z = 0.01$ mm, -124.9 ± 7.2 MPa at $z = 0.03$ mm, and -139.9 ± 7.7 MPa at $z = 0.05$ mm, respectively, and peaks for σ_{yy} at -152.4 ± 6.7 MPa at $z = 0.01$ mm, -164.0 ± 7.4 MPa at $z = 0.01$ mm, and -122.4 ± 7.7 MPa at $z = 0.05$ mm, respectively. In other words, in the σ_{xx} -direction, the z and magnitude of the maximum compressive RS monotonically increased, while, in the σ_{yy} -direction, the z of the maximum compressive RS increased for $f_z = 0.2$ mm, and the magnitude increased to $f_z = 0.1$ mm and then decreased. Tang et al. performed milling on 7050-T7451 and showed that tangential and axial forces increase with increasing f_z and that the maximum RS occurs at a greater z for both σ_{xx} and σ_{yy} RS components from XRD methods [36]. Denkena et al. measured the RS of the σ_{xx} component after milling using the $\sin^2(\psi)$ method and found that as f_z increased, the tangential and axial forces increased, and the maximum compressive RSs

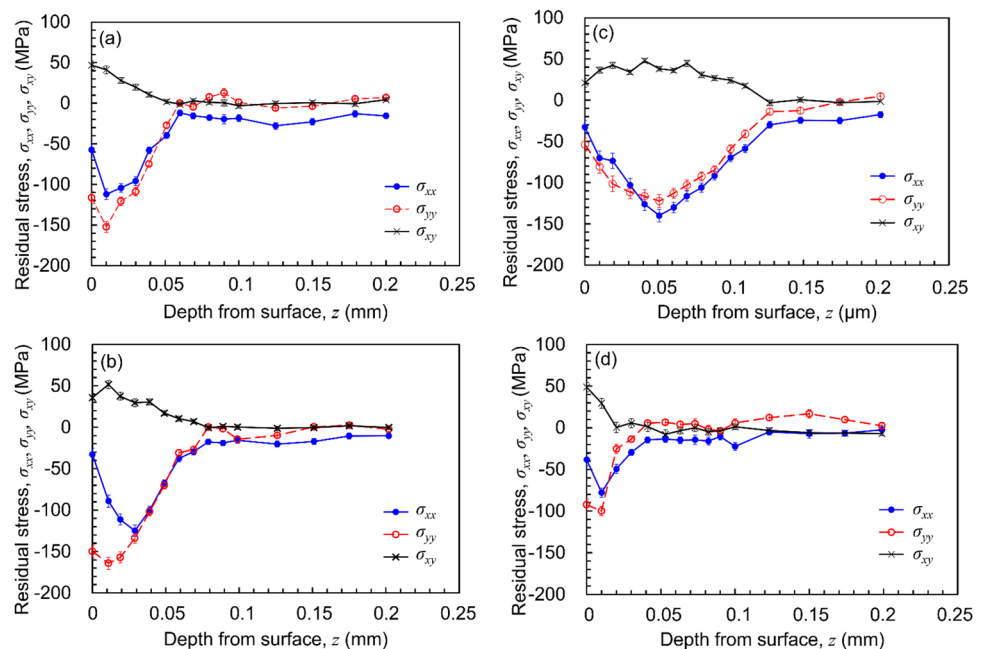
became increasingly deeper and larger [15]. These results are similar to those of the present study. The RSs values in the σ_{yy} -direction were compared using various measurement methods [24]. Although the RSs occurred at greater z values with increasing f_z , the z and magnitudes of the RS peaks differed for each measurement method owing to large measurement errors. However, as shown in Fig. 7, the 2D method has a smaller measurement error, enabling the relative evaluation of the f_z -dependent compressive RS peaks for the σ_{xx} and σ_{yy} components. This indicates that the 2D method can be used to investigate the RS distribution in greater detail than conventional measurement methods. Comparing the maximum values of σ_{xx} and σ_{yy} measured by the 2D method reveals that the maximum compressive RS in Fig. 7a and b with $f_z \leq 0.1$ mm was larger for σ_{yy} than for σ_{xx} . As shown in Fig. 7c, with $f_z = 0.2$ mm, σ_{xx} was slightly larger than σ_{yy} , but σ_{xx} and σ_{yy} showed similar RS distributions in terms of peak position and magnitude.

In milling, machining is performed while the tool rotates; therefore, if the tool is scanned in the x -direction, machining is preferentially performed in the y -direction, which is the direction of the rotational circumference of the tool. Furthermore, if v_c and the number of flutes Z of the tool remain the same, f_z is determined by the number of tool revolutions n , as expressed in Eqs. (9), and n decreases as f_z increases.

$$v_c = f_z \times Z \times n \tag{9}$$

When f_z is small and n is large, the blade is fed in the x -direction after cutting in the y -direction is completed with each rotation of the blade. However, when f_z is large and n is small, cutting in the y -direction is not completed when

Fig. 7 RS near the surface measured via the 2D method: **a** Mode 1, **b** Mode 2, **c** Mode 3, and **d** Mode 4



the blade makes one rotation, and cutting in the x -direction is performed simultaneously. Hence, σ_{xx} increases as f_z increases. Therefore, in Mode 3, with $f_z=0.2$ mm, n was insufficiently predicted, resulting in almost the same amount of cutting in the x - and y -directions each time the blade rotated, and σ_{xx} and σ_{yy} had close distributions. This implies that the values of σ_{xx} and σ_{yy} are predicted to be dependent on the amount of cutting in each stress component direction. Thus, σ_{xx} was larger in the deeper range than in Modes 1 and 2 because the amount of cutting in the shear direction was inevitably larger in Mode 3. In other words, the greater the amount of cutting of each stress component, the greater z and magnitude of the $\sqrt{\quad}$ shape peak, and the deeper the RS distribution. As shown in Fig. 4, the milled surface roughness worsened as f_z increased. A compressive RS is preferred because it suppresses crack propagation. However, considering surface roughness, f_z should not increase.

To investigate the effect of v_c , Modes 1 and 4 were compared, as shown in Fig. 7a and d, where f_z was constant at 0.04 mm and only v_c was changed. The RS z ranges for all stress components were $z \leq 0.06$ mm for Mode 1 with $v_c=200$ m/min and $z \leq 0.04$ mm for Mode 4 with $v_c=450$ m/min, indicating that the larger v_c , the shallower the range of RS. Although the maximum depth of compressive RS in the $\sqrt{\quad}$ shape for both σ_{xx} and σ_{yy} remained the same at $z=0.01$ mm, the values were significantly different: -112.1 ± 6.7 MPa for σ_{xx} and -152.4 ± 6.7 MPa for σ_{yy} in Mode 1, and -77.9 ± 5.4 MPa for σ_{xx} and -100.0 ± 5.4 MPa for σ_{yy} in Mode 4. Tang et al. showed that the tangential force decreases with increasing v_c and that the axial force peaks at a certain v_c [36]. As a result, σ_{xx} and σ_{yy} RS components change to tensile RS at $z=0$ mm with

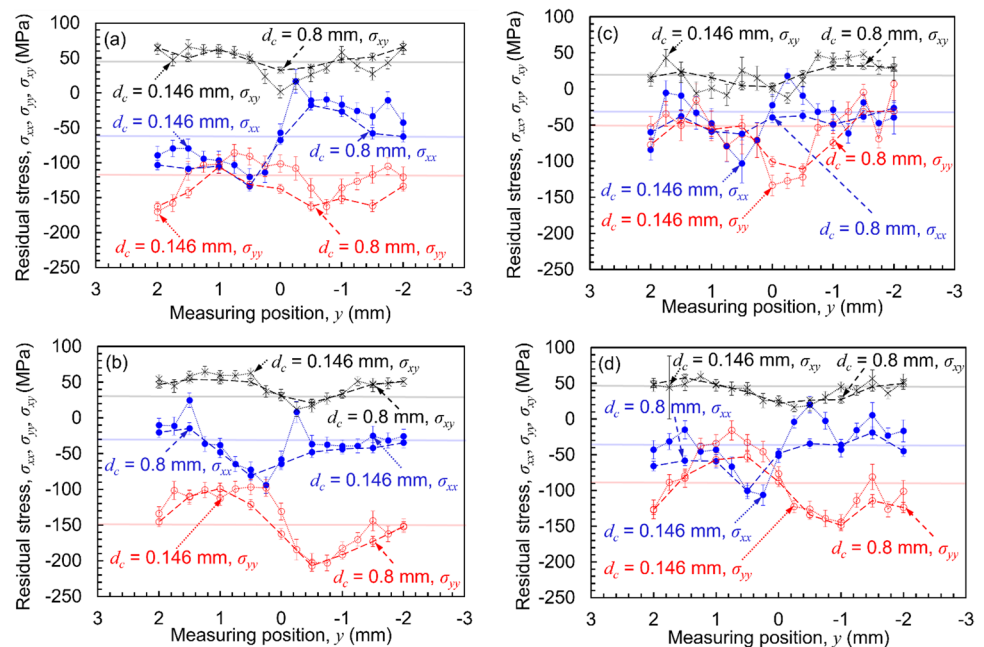
increasing v_c . Denkena also showed that only the tangential force decreases as v_c increases, whereas the axial force remains constant [15], suggesting that the compressive RS value may be smaller and its range shallower because of the decrease in the cutting force as v_c increases. However, Mode 4 is considered a better milling condition because machining is completed at a speed 2.25 times faster than in Mode 1, resulting in higher machining efficiency and small surface roughness, as shown in Fig. 4.

3.4 Effect of the milling parameters on the RS in-plane distribution using the 2D method

Figure 8a–d show the RS distributions in the y -axis direction in the xy -plane at $z=0$ mm measured using the 2D method for samples milled under Modes 1–4. The error bars indicate the standard deviations. To investigate the RS distribution in a 4-mm area set at a_e , the y -axis origin was set as the edge of each milling path, and measurements were conducted in the range of $-2 \text{ mm} \leq y \leq 2 \text{ mm}$. The short and long dotted lines in the figure indicate the results measured using collimators with $d_c=0.146$ and 0.8 mm, respectively. For reference, the average RS values for each stress component at $z=0$ mm in Fig. 7 are indicated by the thin horizontal lines in Fig. 8.

Focusing on the difference in collimator d_c , a RS distribution with a similar trend was obtained for all stress components for both collimators, clearly indicating the existence of an RS distribution in the plane direction as well as a change with z . Nevertheless, a relatively smooth sinusoidal distribution was observed for the collimator with $d_c=0.8$ mm, while several extreme values appeared for the collimator with $d_c=0.146$ mm. All RS measurement methods using XRD

Fig. 8 Surface RSs from the 2D method for each milling condition: **a** Mode 1, **b** Mode 2, **c** Mode 3, and **d** Mode 4



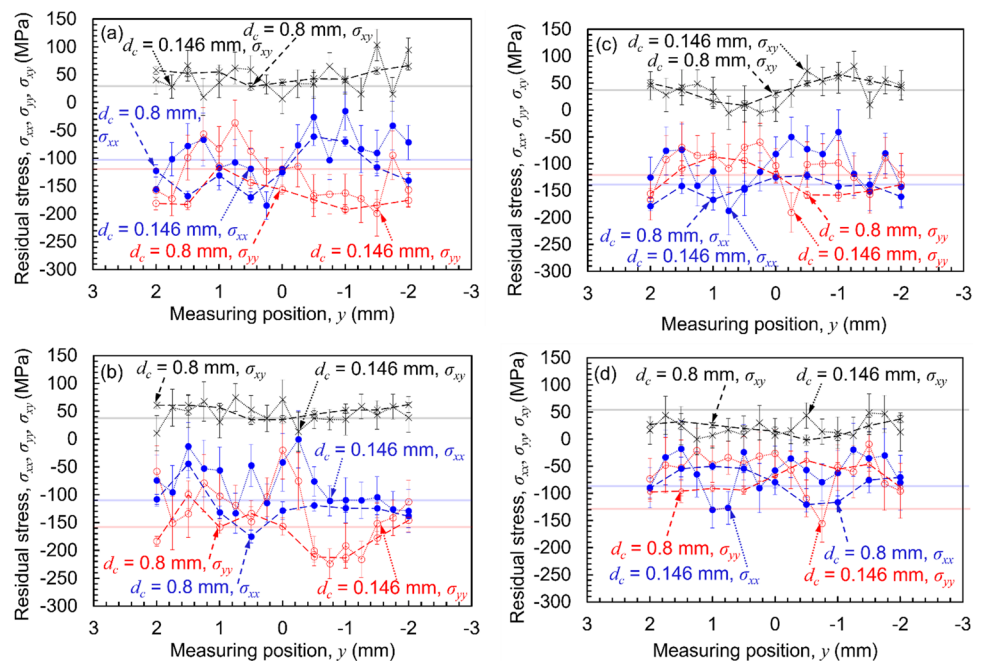
provided averaged diffraction information from the grains in the X-ray-irradiated area. A larger d_c reflects diffraction information from a larger number of crystals, providing results with less variation, whereas a smaller d_c provides a higher spatial resolution. The AA7050-T7451 alloy changed from 1-mm pancake-shaped grains to 1–5- μm fine grains because of the frictional heat from strong machining [37]. Therefore, even with a collimator with $d_c = 0.146$ mm, sufficient diffraction information from the crystals is expected to be obtained because grain refinement caused by strong friction occurs on the machined surface during milling. As evidence, the standard deviation values of the measurement results for $d_c = 0.146$ mm in Fig. 8 are almost the same as those for $d_c = 0.8$ mm, which means that the measurement accuracy for the method at $d_c = 0.146$ mm is sufficiently high. Especially for σ_{xx} , all milling conditions in Modes 1–4 have extreme values of RS near $y = -1.5, -0.25, 0.25,$ and 1.5 mm. Such regular and equally spaced extreme values of RS are caused by a locally strong RS, depending on the tool geometry and other factors.

The RS distribution trend in the xy -plane at $z = 0$ mm was also evaluated. For σ_{xx} , the compressive RS values distributed in the range of $y \geq 0$ mm were greater than in the range of $y \leq 0$ mm for Mode 1 with $f_z = 0.04$ mm and $v_c = 200$ m/min. For Modes 2 and 3 with $f_z \geq 0.1$ mm and Mode 4 with $v_c = 450$ m/min, the compressive RS at $y \geq 0$ mm was smaller than that of Mode 1. Although few studies have been conducted on the RS distribution in the plane direction after milling, Wang et al. investigated the effects of v_c and f_z on the milled surface RS of Al-based composites and evaluated the average RS of σ_{xx}

at three locations on the milled surface using the $\sin^2\psi$ method [11]. They found that when the axial z of the cut was 0.1 mm, the compressive RS decreased with increasing f_z for $v_c \leq 350$ m/min and increased with increasing f_z for $v_c \geq 350$ m/min [11]. Thus, it was reported that the RS distribution on the milled surface depends on the milling parameters. However, for the Mode 4 condition of $v_c = 450$ m/min in this study, the opposite result was observed. Nevertheless, as shown in Fig. 8, the RS values vary significantly depending on the measurement location, even in the same plane. Therefore, to obtain an accurate trend, it is necessary to show the results for each measurement location rather than the average value. The compressive RS of σ_{yy} tended to be smaller for $y > 0$ mm and greater for $y < 0$ mm regardless of the milling conditions. The compressive RS value was particularly small under Modes 3 and 4, indicating that the σ_{yy} stress component decreased as the f_z threshold was exceeded or as v_c increased. Finally, σ_{xy} showed a minimum value at $-0.5 \text{ mm} \leq y \leq 0$ mm for all milling conditions, and the RS decreased as f_z increased, but no significant difference in RS distribution occurred with changes in v_c .

Figure 9a–d show the y -axis direction RS distributions in the xy -plane near z , where the maximum compressive RS occurred, for samples milled in Modes 1–4. The error bars indicate the standard deviations. The evaluated xy -planes were exposed by electropolishing, and the RS in the xy -planes of $z = 20, 20, 50,$ and $14 \mu\text{m}$ were evaluated for Modes 1–4. The average RS values for each stress component at each z shown in Fig. 7 are indicated by thin horizontal lines in Fig. 9.

Fig. 9 In-plane RS at maximum compressive RS z values of each milling condition: **a** Mode 1, **b** Mode 2, **c** Mode 3, and **d** Mode 4



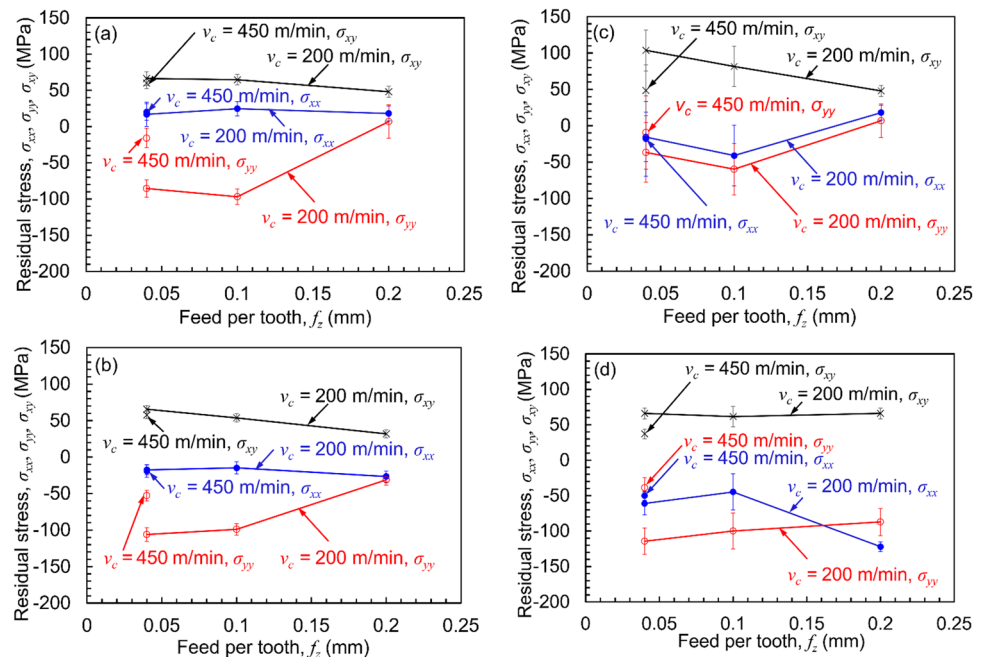
Compared with Fig. 8, which shows the measurement results at $z=0$ mm, many evaluation points have significantly different values owing to the difference in the d_c . In the xy -plane at $z=0$ mm, the tool was in direct contact with the sample; therefore, the in-plane RS distribution trend remained almost the same, even when d_c was different. By contrast, as shown in Fig. 9, the RS distribution changed in a complex manner as the z increased from the milled surface, and the collimator with $d_c=0.8$ mm could not detect the change, whereas the collimator with $d_c=0.146$ mm, which had a higher spatial resolution, showed that the RS distribution significantly. The results in Fig. 8 show that the measurement at $d_c=0.146$ mm is accurate. Comparing the standard deviations in Fig. 9, the standard deviations of $d_c=0.146$ mm is larger than $d_c=0.8$ mm, showing that the local RS values in the xy -plane with $z>0$ vary. Moreover, some regularities were observed in the RS distribution on the machined surface, as shown in Fig. 8, and it is difficult to detect this regularity, as shown in Fig. 9. Therefore, the degrees of tensile RS that could cause fatigue fractures at each z were compared.

Figure 10a and b show the maximum tensile RSs in the xy -plane at $z=0$ mm shown in Fig. 8 for collimators with $d_c=0.146$ and 0.8 mm, respectively, and the error bars indicate the standard deviations. Figure 10c and d show the maximum tensile RSs in the xy -plane near the z -axis, where the maximum compressive RSs are shown in Fig. 9 for collimators with $d_c=0.146$ and 0.8 mm.

Initially, the effect of v_c at $z=0$, as in Fig. 10a and b, showed that for both collimators, σ_{xx} remained almost unchanged with increasing v_c , while σ_{yy} changed

significantly to the tensile side, and σ_{xy} became slightly smaller. The effect of f_z was almost the same for σ_{xx} as f_z increased, whereas σ_{yy} showed a large tensile change and σ_{xy} showed a slightly decreasing trend. When a collimator with $d_c=0.146$ mm was used, σ_{xx} showed tensile RS for all conditions, while σ_{yy} showed tensile RS only in Mode 4. For the collimator with $d_c=0.8$ mm, σ_{xx} and σ_{yy} are compressive RSs. In the near- z region, as shown in Fig. 10c and d, where the maximum compressive RS occurred, the changing trend in values differed for each collimator. For the collimator with $d_c=0.146$ mm, σ_{xx} remained almost unchanged with increasing v_c , while σ_{yy} changed slightly to the tensile side, and σ_{xy} became much smaller. The effects of f_z , σ_{xx} , and σ_{yy} showed a maximum compressive RS at $f_z=0.1$ mm. It then changed significantly to the tensile side at $f_z=0.2$ mm, and σ_{xy} decreased monotonically. The values of σ_{xx} and σ_{yy} showed tensile RS only in Mode 4. By contrast, for the collimator with $d_c=0.8$ mm, σ_{xx} changed slightly to the tensile side, and σ_{yy} changed significantly to the tensile side with increasing v_c , whereas σ_{xy} became smaller. For the effect of f_z , σ_{xx} showed a minimum compressive RS at $f_z=0.1$ mm and then changed significantly to the compressive side at $f_z=0.2$ mm, while σ_{yy} changed monotonically to the tensile side with increasing f_z , and σ_{xy} remained almost unchanged. As in the case of $z=0$ mm, σ_{xx} and σ_{yy} are the compressive RS components. These results show that in the xy -plane at the z where the maximum compressive RS occurred, the effects of the different collimators were significant, especially for σ_{xx} at $f_z=0.2$ mm. These differences result from the difference in spatial resolution for the collimators, and the collimator with $d_c=0.8$ mm averaged RSs over a larger

Fig. 10 Relationship between milling conditions and maximum RS on the xy -plane: **a** $z=0$ mm, $d_c=0.146$ mm, **b** $z=0$ mm, $d_c=0.8$ mm, **c** maximum compressive RS z at $d_c=0.146$ mm, and **d** maximum compressive RS z at $d_c=0.8$ mm



area, which may have prevented detailed values from being obtained for the local area.

In summary, tensile RSs are more likely to occur at σ_{xx} on a surface with $z=0$ mm, and tensile RSs that cause fatigue failure are more likely to occur as v_c and f_z increase, regardless of the z . The variation in the RS distribution in the plane direction is directly related to the distortion of thin-plate materials. The machining efficiency is better with larger v_c and f_z ; however, it is necessary to determine the milling conditions that consider the surface precision and RS distribution to improve the fatigue performance. If compressive RS can be introduced by adjusting the milling conditions to suppress the initiation and propagation of fatigue cracks without generating tensile RSs that cause fatigue, aircraft safety can be improved.

4 Conclusions

An AA7050-T7451 aluminum alloy was milled under four feed-per-tooth (f_z) and cutting speed (v_c) conditions, and the RS distributions with z from the surface in the plane direction were measured using a 2D-XRD method. The major findings of this study are as follows.

1. The maximum height roughness (R_z) and arithmetical mean height (R_a) were 3.7 and 0.7 μm when $f_z=0.04$ mm and $v_c=200$ m/min, and changing only f_z to 0.2 mm resulted in R_z and R_a of 25.1 and 3.1 μm , respectively; R_z and R_a were 7.3 and 1.1 μm , respectively, when only v_c was changed to 450 m/min, indicating that the milled surface roughness was affected more by f_z than by v_c .
2. The changes in RS with z after milling were compared using the hole-drilling, slotting, $\sin^2(\psi)$, $\cos(\alpha)$, and 2D methods, and the results agreed well, except for those from the $\cos(\alpha)$ method.
3. The 2D method has a high correlation coefficient (0.973) compared with the hole-drilling method. The 2D method has high repeatability and a small measurement error near the surface, where the hole-drilling method does not perform well. The standard deviation of the RS at $z=0.005$ mm for the 2D method was 7.8 MPa, whereas that for the hole-drilling method was 92.1 MPa.
4. RS changes with z after milling were evaluated using the 2D method. The maximum axial RS (σ_{xx}) and tangential RS (σ_{yy}) at $f_z=0.04$ mm and $v_c=200$ m/min both occurred at $z=0.01$ mm, while $\sigma_{xx}=-112.1 \pm 6.7$ MPa and $\sigma_{yy}=-152.4 \pm 6.7$ MPa occurred at $z=0.01$ mm. By changing only f_z to 0.2 mm, we found $\sigma_{xx}=-139.9 \pm 7.7$ MPa and $\sigma_{yy}=-122.4 \pm 7.7$ MPa at $z=0.05$ mm, and by changing only v_c to 450 m/min, z remained the same at 0.01 mm, resulting in $\sigma_{xx}=-77.9 \pm 5.4$ MPa and $\sigma_{yy}=100.0 \pm 5.4$ MPa. Thus,

the greater the cutting, the greater the z and magnitude of the maximum compressive RS for each component and the deeper the RS distribution. For all stress components, the compressive RS tended to increase with increasing f_z and decreased with increasing v_c .

5. The RSs in the planar direction after milling were measured using the 2D method with two collimator diameters (d_c). The RS distribution on the milled surface exhibited a sinusoidal distribution in the planar direction for both collimators. In particular, the smaller condition ($d_c=0.146$ mm) enabled measurements with a higher spatial resolution.
6. After milling in the plane direction, tensile RSs were more likely to occur on the milled surface, particularly the stress component in the tool feed direction. At any z , the tensile RSs were more likely to occur as v_c and f_z increased. For example, at $z=0$ mm, the maximum $\sigma_{yy}=-85.6$ MPa at $v_c=200$ m/s and $f_z=0.05$ mm, while changing only v_c to 450 m/s resulted in $\sigma_{yy}=-16$ MPa, and changing only f_z to 0.2 mm resulted in $\sigma_{yy}=6.8$ MPa.

Acknowledgements The authors would like to thank Benjamin Kirsch (RPTU Kaiserslautern, Germany), for planning and conceptualization and Daniel Weber (RPTU Kaiserslautern, Germany) for the milling experiments and planning. The authors are deeply grateful to Christopher R. D'Elia (UC Davis, USA), for planning, conceptualizing, procuring material, and reporting. Special thanks also go to Barbara S. Linke (UC Davis, USA) for funding, conceptualization, and organization. This research was partially supported by JSPS KAKENHI, Grant Numbers 18KK0103 and 22KK0050.

Author contributions All authors contributed to the conception and investigation of this study. The methodology was conceived by Christopher R. Chighizola, Michael R. Hill, Jan C. Aurich, and Hitoshi Soyama. All data were visualized using Chieko Kuji software. Hitoshi Soyama supervised this study. The first draft of the manuscript was written by Chieko Kuji, and all authors commented on previous versions of the manuscript. All authors read and approved the final manuscript.

Funding This research was partially supported by JSPS KAKENHI, Grant Numbers 18KK0103 and 22KK0050.

Declarations

Competing interests The authors have no relevant financial or non-financial interests to disclose.

Open Access This article is licensed under a Creative Commons Attribution 4.0 International License, which permits use, sharing, adaptation, distribution and reproduction in any medium or format, as long as you give appropriate credit to the original author(s) and the source, provide a link to the Creative Commons licence, and indicate if changes were made. The images or other third party material in this article are included in the article's Creative Commons licence, unless indicated otherwise in a credit line to the material. If material is not included in the article's Creative Commons licence and your intended use is not permitted by statutory regulation or exceeds the permitted use, you will need to obtain permission directly from the copyright holder. To view a copy of this licence, visit <http://creativecommons.org/licenses/by/4.0/>.

References

- Li JG, Wang SQ (2017) Distortion caused by residual stresses in machining aeronautical aluminum alloy parts: recent advances. *Int J Adv Manuf Technol* 89:997–1012. <https://doi.org/10.1007/s00170-016-9066-6>
- Santos MC, Machado AR, Sales WF, Barrozo MAS, Ezugwu EO (2016) Machining of aluminum alloys: a review. *Int J Adv Manuf Technol* 86:3067–3080. <https://doi.org/10.1007/s00170-016-8431-9>
- Madariaga A, Perez I, Arrazola PJ, Sanchez R, Ruiz JJ, Rubio FJ (2018) Reduction of distortions in large aluminium parts by controlling machining-induced residual stresses. *Int J Adv Manuf Technol* 97:967–978. <https://doi.org/10.1007/s00170-018-1965-2>
- Herbert S, Toshimichi M (1992) High-speed machining. *CIRP Ann Manuf Technol* 41:637–643. [https://doi.org/10.1016/S0007-8506\(07\)63250-8](https://doi.org/10.1016/S0007-8506(07)63250-8)
- Dudzinski D, Devillez A, Moufki A, Larrouquere D, Zerrouki V, Vigneau J (2004) A review of developments towards dry and high speed machining of Inconel 718 alloy. *Int J Mach Tools Manuf* 44:439–456. [https://doi.org/10.1016/s0890-6955\(03\)00159-7](https://doi.org/10.1016/s0890-6955(03)00159-7)
- Brinksmeier E, Sölter J (2009) Prediction of shape deviations in machining. *CIRP Ann Manuf Technol* 58:507–510. <https://doi.org/10.1016/j.cirp.2009.03.123>
- Jiang ZL, Liu YM, Li L, Shao WX (2014) A novel prediction model for thin plate deflections considering milling residual stresses. *Int J Adv Manuf Technol* 74:37–45. <https://doi.org/10.1007/s00170-014-5952-y>
- Bowden DM, Halley J (2001) Aluminium reliability improvement program-final report 60606. The Boeing Company, Chicago
- Elkhabeery MM, Fattouh M (1989) Residual-stress distribution caused by milling. *Int J Mach Tools Manuf* 29:391–401. [https://doi.org/10.1016/0890-6955\(89\)90008-4](https://doi.org/10.1016/0890-6955(89)90008-4)
- Yao CF, Zuo W, Wu DX, Ren JX, Zhang DH (2015) Control rules of surface integrity and formation of metamorphic layer in high-speed milling of 7055 aluminum alloy. *Proc Inst Mech Eng B J Eng Manuf* 229:187–204. <https://doi.org/10.1177/0954405414527268>
- Wang T, Xie LJ, Wang XB, Jiao L, Shen JW, Xu H, Nie FM (2013) Surface integrity of high speed milling of Al/SiC/65p aluminum matrix composites. *Procedia CIRP* 8:475–480. <https://doi.org/10.1177/0954405415573704>
- Weber D, Kirsch B, Chighizola CR, D'Elia CR, Linke BS, Hill MR, Aurich JC (2021) Analysis of machining-induced residual stresses of milled aluminum workpieces, their repeatability, and their resulting distortion. *Int J Adv Manuf Technol* 115:1089–1110. <https://doi.org/10.1007/s00170-021-07171-7>
- Feng Y, Pan Z, Lu X, Liang SY (2018) Analytical and numerical predictions of machining-induced residual stress in milling of Inconel 718 considering dynamic recrystallization. *Proc ASME 2018 13th Int Manuf Sci Eng Conf* 4:V004T03A023. <https://doi.org/10.1115/MSEC2018-6386>
- Feng Y, Hung TP, Lu YT, Lin YF, Hsu FC, Lin CF, Lu YC, Liang SY (2019) Residual stress prediction in laser-assisted milling considering recrystallization effects. *Int J Adv Manuf Technol* 102:393–402. <https://doi.org/10.1007/s00170-018-3207-z>
- Denkena B, Boehnke D, Lde L (2008) Machining induced residual stress in structural aluminum parts. *Prod Eng Res Devel* 2:247–253. <https://doi.org/10.1007/s11740-008-0097-1>
- Masoudi S, Amini S, Saeidi E, Eslami-Chalander H (2015) Effect of machining-induced residual stress on the distortion of thin-walled parts. *Int J Adv Manuf Technol* 76:597–608. <https://doi.org/10.1007/s00170-014-6281-x>
- Li BZ, Jiang XH, Yang JG, Liang SY (2015) Effects of depth of cut on the redistribution of residual stress and distortion during the milling of thin-walled part. *J Mater Process Technol* 216:223–233. <https://doi.org/10.1016/j.jmatprotec.2014.09.016>
- Vaara J, Kunnari A, Frondelius T (2020) Literature review of fatigue assessment methods in residual stressed state. *Eng Failure Anal* 110:104379. <https://doi.org/10.1016/j.engfailanal.2020.104379>
- Otkur M, Lazoglu I (2007) Trochoidal milling. *Int J Mach Tools Manuf* 47:1324–1332. <https://doi.org/10.1016/j.ijmactools.2006.08.002>
- Withers PJ, Bhadeshia H (2001) Overview - residual stress part 1 - measurement techniques. *Mater Sci Technol* 17:355–365. <https://doi.org/10.1179/026708301101509980>
- Kara F, Özbek O, Özbek NA, Uygur İ (2021) Investigation of the effect of deep cryogenic process on residual stress and residual austenite. *Gazi J Eng Sci* 7:143–151. <https://doi.org/10.30855/gmbd.2021.02.07>
- Vrabel M, Eckstein M, Maňková I (2018) Analysis of the metallography parameters and residual stress induced when producing bolt holes in Inconel 718 alloy. *Int J Adv Manuf Technol* 96:4353–4366. <https://doi.org/10.1007/s00170-018-1902-4>
- Bordinassi EC, Mhurchadha SU, Seriacopi V, Delijaicov S, Marraccini S, Lebrão G, Thomas K, Batalha GF, Raghavendra R (2022) Effect of hybrid manufacturing (am-machining) on the residual stress and pitting corrosion resistance of 316L stainless steel. *J Braz Soc Mech Sci Eng* 44:491. <https://doi.org/10.1007/s40430-022-03813-3>
- Chighizola CR, D'Elia CR, Weber D, Kirsch B, Aurich JC, Linke BS, Hill MR (2021) Intercomparison and evaluation of measured near surface residual stress in milled aluminum. *Exp Mech* 61:1309–1322. <https://doi.org/10.1007/s11340-021-00734-5>
- Soyama H, Kuji C, Kuriyagawa T, Chighizola CR, Hill MR (2021) Optimization of residual stress measurement conditions for a 2D method using X-ray diffraction and its application for stainless steel treated by laser cavitation peening. *Mater* 14:2772. <https://doi.org/10.3390/ma14112772>
- Weber D, Kirsch B, Chighizola CR, Jonsson JE, D'Elia CR, Linke BS, Hill MR, Aurich JC (2020) Finite element simulation combination to predict the distortion of thin walled milled aluminum workpieces as a result of machining induced residual stresses. *iPMVM 2020* 89:11:1–11:21. <https://doi.org/10.4230/OASICS.iPMVM.2020.11>
- ASTM International - ASTM E837–20 (2013) Standard test method for determining residual stresses by the hole-drilling strain-gage method. West Conshohocken, PA
- Liu CG, Zheng Y, Zhang XG (2017) Investigation of through thickness residual stress distribution and springback in bent AL plate by slotting method. *Int J Adv Manuf Technol* 90:299–308. <https://doi.org/10.1007/s00170-016-9322-9>
- Olson MD, Watanabe BT, Wong TA, DeWald AT, Hill MR (2022) Near surface residual stress measurement using slotting. *Exp Mech* 62:1401–1410. <https://doi.org/10.1007/s11340-022-00858-2>
- DIN EN 15305:2009 (2009) Non-destructive testing. Test method for residual stress analysis by X-ray diffraction. Berlin
- Lodh A, Thool K, Samajdar I (2022) X-ray diffraction for the determination of residual stress of crystalline material: an overview. *Trans Indian Inst Met* 75:983–995. <https://doi.org/10.1007/s12666-022-02540-6>
- Tanaka K (2019) The $\cos\alpha$ method for X-ray residual stress measurement using two-dimensional detector. *Mech Eng Rev* 6:18–00378. <https://doi.org/10.1299/mer.18-00378>

33. Rossini NS, Dassisti M, Benyounis KY, Olabi AG (2012) Methods of measuring residual stresses in components. *Mater Des* 35:572–588. <https://doi.org/10.1016/j.matdes.2011.08.022>
34. He BB (2009) Two-Dimensional X-ray Diffraction. John Wiley & Sons, Hoboken, NJ
35. Luo Q, Jones AH (2010) High-precision determination of residual stress of polycrystalline coatings using optimised XRD- $\sin^2\psi$ technique. *Surf Coat Technol* 205:1403–1408. <https://doi.org/10.1016/j.surfcoat.2010.07.108>
36. Tang ZT, Liu ZQ, Wan Y, Ai X (2008) Study on residual stresses in milling aluminium alloy 7050-T7451. Yan XT, Jiang C, Eynard B. (eds) *Advanced Design and Manufacture to Gain a Competitive Edge*. https://doi.org/10.1007/978-1-84800-241-8_18
37. Jata KV, Sankaran KK, Ruschau JJ (2000) Friction-stir welding effects on microstructure and fatigue of aluminum alloy 7050-T7451. *Metall Mater Trans A Phys Metall Mater Sci* 31:2181–2192. <https://doi.org/10.1007/s11661-000-0136-9>

Publisher's note Springer Nature remains neutral with regard to jurisdictional claims in published maps and institutional affiliations.